Renewable Energy 239 (2025) 122122

Contents lists available at ScienceDirect

Renewable Energy

journal homepage: www.elsevier.com/locate/renene

Enhanced methanol tolerance of ZIF-8-immobilized *Aspergillus oryzae* lipase for biodiesel production from used cooking oil

Shuaibo Xia [a], Cai Shen [b,**], Jiale Lin [a], Maolin Tu [a], Chin-Ping Tan [c], Ling-Zhi Cheong [b,*]

[a] Zhejiang-Malaysia Joint Research Laboratory for Agricultural Product Processing and Nutrition, College of Food and Pharmaceutical Science, Ningbo University, Ningbo, 315211, China
[b] School of Agriculture, Food and Ecosystem Sciences, Faculty of Science, University of Melbourne, Australia
[c] Department of Food Technology, Faculty of Food Science and Technology, University Putra Malaysia, Serdang, Selangor, 43400, Malaysia

ARTICLE INFO

Keywords:
Molecular dynamic simulation
Lipase immobilization
Biodiesel
Zeolitic imidazolate frameworks

ABSTRACT

The absorption process of *Aspergillus oryzae* lipase (AOL) onto the surface of ZIF-8 was elucidated using molecular dynamic (MD) simulation. AOL are absorbed onto the surface of ZIF-8 via hydrogen bonding, electrostatic and van der Waals interaction with minimal changes to its native configurations. Unlike free AOL, AOL@ZIF-8 can maintain its structure in simulated methanol solutions. To verify the results from MD simulation, AOL was immobilized onto ZIF-8 (AOL@ZIF-8: immobilization efficiency of 64.71 % and a protein loading of 57.36 mg/g) and characterized using SEM, FTIR, and XRD. As compared to free AOL, AOL@ZIF-8 demonstrated higher transesterification activity with an activity recovery of 106.18 %. In agreement with MD simulations, AOL@ZIF-8 exhibited enhanced stability in wide range of pH and under presence of alcohol solution. AOL@ZIF-8 can be used to catalyze transesterification of used cooking oil for production of biodiesel (FAME content of 81.19 %).

1. Introduction

Biodiesel, comprised of various fatty acid methyl esters (FAME) or fatty acid ethyl esters (FAEE), is increasingly recognized as a viable solution to reduce global reliance on fossil fuels [1]. Biodiesel can be synthesized by transesterification of triglycerides from various sources including used cooking oil, jatropha oil, and algal oil, with short-chain alcohols such as methanol or ethanol. This process is usually catalyzed by acid and basic catalysts, as well as biocatalysts. Acid catalysts like sulfuric acid or hydrochloric acid are corrosive and requires high reaction temperature and pressure. Chemical catalysts also present other drawbacks such as waste generation, and potential side reactions [2].

Lipase-catalyzed transesterification has garnered attention due to its high specificity, mild reaction conditions (reaction temperature: 40–60 °C, reaction time: 12–24 h, pH: 6.0–8.0) and ease of product separation. Lipases reacts with triglycerides or free fatty acids to form a covalently modified enzyme (acyl-enzyme), which subsequently reacts with alcohol to produce alkyl esters [3]. Nonetheless, challenges exist in terms of lipase inactivation by substrates with high acidity and short-chain alcohols. Immobilization technology, which involves physical confinement or localization of enzymes within a defined region of space while retaining their catalytic activities, can be used to overcome this limitation [4].

Zeolitic imidazolate frameworks (ZIF) offer promising prospects for enzyme immobilization due to their mild synthesis conditions, non-toxicity, large specific surface area, diverse morphology, and excellent chemical stability [5]. We have successfully synthesized various ZIF structures with distinct pore architectures for lipase immobilization which resulted in enhanced catalytic activity (hydrolytic, esterification and transesterification activity), catalytic stability in harsh conditions (presence of alcohol and denaturants) and reusability as compared to free lipase [6–8]. Thus, ZIF-immobilized lipases have great potential for production of biodiesel. Some works have used ZIF-immobilized lipase in the preparation of biodiesel. Zha et al. applied entrapment immobilization of lipase in ZIF-8 as catalyst in biodiesel production. An approximate 75 % biodiesel yield was achieved and 80 % of initial activity was remained after five cycles of transesterification [9]. Giraldo et al. used adsorbed *Candida Antarctica* Lipase B on ZIF-8 to synthesize biodiesel and the system presented 95 % biodiesel conversion [10].

Molecular dynamics (MD) simulations offer a valuable tool for predicting the dynamic behavior of atoms over time, encompassing phenomena such as conformational changes, ligand binding, and protein

* Corresponding author.
** Corresponding author.
E-mail addresses: cai.shen@unimelb.edu.au (C. Shen), lingzhi.cheong@unimelb.edu.au (L.-Z. Cheong).

https://doi.org/10.1016/j.renene.2024.122122
Received 5 June 2024; Received in revised form 12 November 2024; Accepted 7 December 2024
Available online 7 December 2024

folding [11]. MD simulations can be used to elucidate the microscopic mechanisms underlying the adsorption of lipase onto carrier surfaces. Zhao et al. elucidated the orientation and adsorption mechanism of lipase on the surfaces of four distinct nanomaterials with varying surface chemical properties, including hydrophobic graphite, hydrophilic TiO_2, and surfaces with positive and negative charges [12]. Their simulation outcomes revealed strong lipase adsorption onto hydrophobic surfaces, while lipase molecules tended to orient their catalytic centers towards the solution when adsorbed onto negatively charged surfaces. These findings demonstrate MD simulations can be used to understand and optimize lipase immobilization processes.

This study aims to investigate and elucidate the adsorption behavior of free lipase from *Aspergillus oryzae* (AOL) onto the ZIF-8 surface and to assess the methanol tolerance of ZIF-8-immobilized lipase (AOL@ZIF-8) in methanol solution using MD simulations. The MD simulation results were verified experimentally by assessing the catalytic stability of ZIF-8-immobilized lipase following methanol treatment. Furthermore, the catalytic activity and stability of ZIF-8-immobilized lipase under harsh reaction conditions were evaluated. The ZIF-8 immobilized lipase was then used to synthesis biodiesel from used cooking oils. Result from this study will provide valuable guidance for development of stable and robust immobilized lipases for valorization of used cooking oil.

2. Materials and methods

2.1. Materials

Aspergillus oryzae lipase was generously provided by Novozyme. 2-Methylimidazole (98 %), $Zn(NO_3)_2{\cdot}6H_2O$, p-NPP (98 %), methanol (99.5 %), ethanol (99.7 %), n-hexane (97 %) and methyl heptadecanoate (99 %) were purchased from Aladdin and Macklin Chemicals. Sunflower oil was obtained from a local market in Ningbo, China. Fatty acid methyl ester standard, product number BYG8010, purchased from Solarbio; n-hexane, chromatographic grade, purchased from Macklin Reagent; methyl heptadecanoate internal standard, chromatographic grade, purchased from Solarbio; methanol, ethanol, isopropanol, anhydrous sodium sulfate, sodium hydroxide, potassium hydroxide, hydrochloric acid standard titration solution, sodium hydroxide standard titration solution, sodium thiosulfate standard titration solution, chloroform, ether, glacial acetic acid, phenolphthalein, potassium iodide, and soluble starch, all purchased from Macklin or Solarbio, are all of analytical grade [7].

2.2. Molecular dynamics simulation

The adsorption behavior of AOL (PDB ID:5XK2) onto ZIF-8 was investigated using GROMACS 2021.5 package. AOL was parameterized by Amberff14sb force field [13]. The AMBER-compatible force field parameters and partial charges of ZIF-8 were constructed according to previously published method [14]. The ZIF-8 framework consists of 6 × 6 × 1 unit cells (area = 10.8 × 10.8 nm^2 in x and y direction and with a total of 16464 atoms) was placed at the bottom of the simulation box (12.5 × 12.5 × 12.5 nm^3) with an initial distance of more than 1.4 nm from the AOL. The system was solvated in TIP3P water, and 5 Na^+ ions were added to keep the system electrically neutral. Energy minimization was performed using the steepest descent algorithm with a force tolerance of 500 kJ mol^{-1} nm^{-1}. Periodic boundary conditions were imposed in all the three directions. System was pre-balanced for 1 ns under NVT ensemble from 0 to 310 K and relaxed for 1 ns under NPT ensemble, performing a constant of 1000 kJ mol^{-1} nm^{-2} position constraints on heavy atoms of ZIF-8 and lipase in three directions. After completing the above steps, 100 ns MD simulations were performed with a time step of 2 fs and heavy atoms of ZIF-8 was restrained. Pressure was maintained at 1 bar by the Parrinello-Rahman barostat in an semi-isotropic manner (x, y and z directions) and temperature was maintained at 310 K by the V-rescal thermostat [15,16]. The LINCS algorithm was performed for constrain bond lengths of hydrogen atoms. Lennard-Jones interactions were calculated within a cutoff of 1.2 nm, and electrostatic interactions beyond 1.2 nm were treated with particle-mesh Ewald (PME) method with a grid spacing of 0.16 nm. UCSF ChimeraX was used to visualize all results.

Methanol tolerance of AOL@ZIF-8 was investigated using GROMACS 2021.5 package. The structure of lipase@ZIF-8 was obtained by MD simulation in the previous step was taken as the initial conformation and free lipase was used as controls. Methanol was geometrically optimized by Gaussian 16 (Revision A.03) under SMD (water) implicit solvation model with density functional theory B3LYP-D3(BJ)/def-TZVP level. AmberTools21 and ACPYPE were used to construct the general AMBER force field 2 (GAFF2) parameters [17,18], Multiwfn was used to fit the restrained electrostatic potential 2 (RESP2) charge [19,20].

2.3. Synthesis of ZIF-8

ZIF-8 was synthesized following our previously published method with slight modifications [7]. Specifically, 2-methylimidazole (2.8375 g) was dissolved in 50 mL $Zn(NO_3)_2{\cdot}6H_2O$ solution (0.1475 g in 50 mL deionized water) and stirred for 30 min at room temperature. The mixture was centrifuged at 10,000 rpm and washed three times with deionized water. The resulting white solids were vacuum-dried overnight at 50 °C and subsequently ground to obtain ZIF-8.

2.4. Immobilization of AOL onto ZIF-8

ZIF-8 (40 mg) was dispersed in 2 mL of deionized water using a sonicator. Subsequently, a solution of AOL (2 mL, 5 mg/mL) was added to the ZIF-8 suspension, followed by magnetic stirring at 200 rpm for 8 h at 37 °C. The resulting immobilized lipase (AOL@ZIF-8) was collected via centrifugation, washed three times with deionized water, and dried overnight. Protein concentrations in the immobilized lipase were determined using the BCA Protein Assay Kit, and the immobilization efficiency was calculated using Equation (1):

$$\text{Immobilization efficiency} = \frac{c_0\text{-}c_1}{c_0} \times 100\% \quad (1)$$

where c_0 and c_1 represent the protein concentrations of lipase solution and supernatant after centrifugation, respectively.

2.5. Characterization of ZIF-8 and AOL@ZIF-8

The structure of ZIF-8 and AOL@ZIF-8 was characterized using powder X-ray diffraction (XRD) (Bruker D8 Discover XRD, Cu radiation, λ = l.540596 Å) and fourier transform infrared spectroscopy (FTIR; FT/IR-4700 type A, Japan). Peakfit software was used to perform baseline correction, Gaussian deconvolution and second derivative fitting for the FTIR spectra, and then the content of each secondary structure was calculated according to the peak area. Scanning electron microscope (SEM; S4800, Hitachi, Japan) was used to observe microscopic morphology. Specific surface area and pore size were determined through Brunauer-Emmett-Teller (BET; Quantachrome Autosorb IQ3, USA) method and nitrogen adsorption-desorption plot. Thermal gravimetric analyses (TGA) were measured using TG 209F1 Libra (NETZSCH, Germany) from 30 °C to 800 °C at a heating rate of 20 °C/min [21].

2.6. Catalytic activity and stability of AOL@ZIF-8

The catalytic activity and stability of AOL@ZIF-8 were evaluated through transesterification of p-nitrophenol palmitate (p-NPP) with ethanol [22]. Specifically, 1 mL of p-NPP was dissolved in n-hexane (10 mM) and mixed with 60 μL of ethanol. Subsequently, AOL@ZIF-8 or free AOL (0.1 mg) was added to the substrate mixture, and the transesterification reaction was carried out in an incubator shaker at 40 °C for

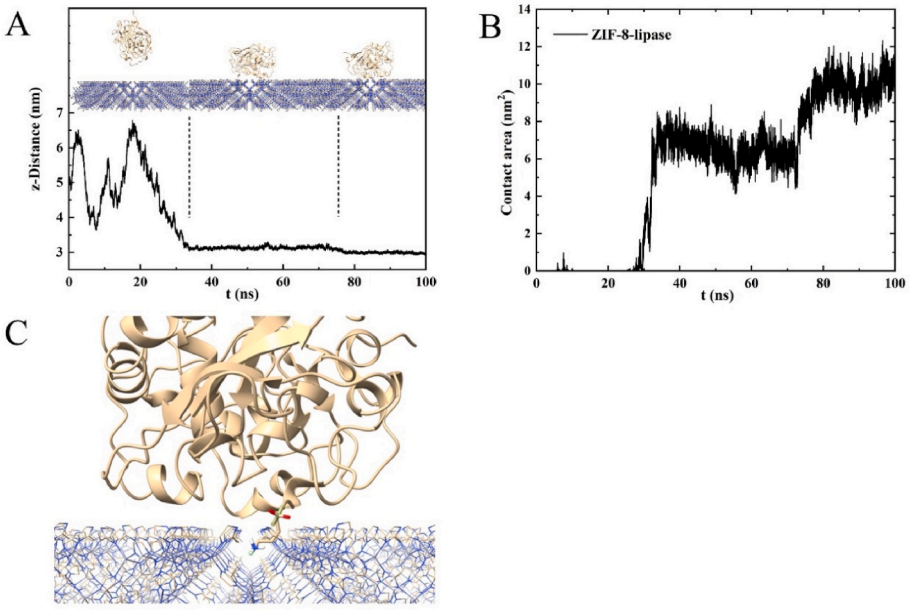

Fig. 1. z-Distance (A) and contact area (B) between AOL and ZIF-8; MD simulations of AOL and ZIF-8 at 75 ns (C).

20 min at 200 rpm. The reaction was terminated by adding 1 mL of 0.1 M NaOH solution. p-NP (p-nitrophenol, a by-product of the reaction) was extracted from the reaction mixture by centrifugation at 10,000 rpm for 10 min and detected at an absorbance wavelength of 410 nm. Transesterification activity was quantified as the amount of lipase required to produce 1 μmol of p-NP per minute, and activity recovery was calculated as the ratio of the transesterification activity of immobilized lipase to free lipase. The concentration of p-NP was determined using a p-NP standard curve ($Y = 11.6061X - 0.02749$, $R^2 = 0.9979$). The kinetic parameters (Km and Vmax) of free AOL and AOL@ZIF-8 were determined by transesterification of p-NPP at various concentrations (0.45, 0.9, 1.8, 3.6, 7.2, 14.4 mM) for the same reaction time. These parameters were calculated using the Michaelis−Menten equation.

The catalytic stability of AOL@ZIF-8 was assessed by measuring the transesterification activity following pre-treatment of AOL@ZIF-8 solutions (1 mg/mL in deionized water) under various conditions. This included exposure to different temperatures (ranging from 40 °C to 90 °C for 30 min), pH levels (ranging from pH 5.0 to 9.0 for 1 h), and solvent compositions (methanol and ethanol solutions, ranging from 5 % to 30 %, v/v for 1 h).

2.7. AOL@ZIF-8-catalyzed biodiesel production from used cooking oil

2.7.1. Effects of frying time on the acid value, peroxide value and total polar compound of used cooking oils

Fresh oil was used to fry chicken nuggets at 180 °C repeatedly for 12 h. Oil samples were collected at every hour, filtered through filter paper to remove food residue, and used for determination of acid value, peroxide value and total polar compound.

For determination of acid value (AV), oil samples (1–3 g) were dissolved in mixture of ether and isopropanol (1:1, v/v, 50 mL). Following that, 3–4 drops of phenolphthalein indicator were added. Titration was performed using NaOH standard titrant solution until a faint pink color appeared in the solution. A blank control was performed simultaneously. The AV of the oil was calculated using Equation (2):

$$AV = \frac{(v\text{-}v_0) \times c \times 56.1}{m} \quad (2)$$

where V and V_0 represent the volume of NaOH used in the experimental and blank groups, respectively; c is the concentration of the NaOH titration solution used; and m is the mass of the oil sample.

To determine peroxide value, the oil sample (1–3 g) was dissolved in a mixture of chloroform and glacial acetic acid (30 mL, 2:3 v/v). One milliliter of saturated potassium iodide solution was added to the mixture, gently shake for 30 s and placed in dark for 3 min. Following that, 100 mL of deionized water was added to the mixture and titrated using $Na_2S_2O_3$ standard titrant solution until formation of a faint yellow color in the solution. One milliliter of starch indicator solution was added to the solution which turned into blue color. The titration was continued until the blue color disappeared. The volume of $Na_2S_2O_3$ standard titrant solution used was recorded as V, and the blank control group was recorded as V_0. Peroxide value (PV) of the oil was calculated using Equation (3):

$$PV = \frac{(v\text{-}v_0) \times c \times 0.1269}{m} \times 100 \quad (3)$$

where V and V_0 represent the volume of $Na_2S_2O_3$ used in the experimental and blank groups, respectively; c is the concentration of the $Na_2S_2O_3$ standard titrant solution used; and m is the mass of the oil sample.

Total polar compound (TPC) content was conducted according to the following method. Silica gel (10 g) was filled into a glass chromatography column (40 × 1 cm). Oil sample (0.5 g) was dissolved in n-hexane and loaded onto the column. Non-polar compounds were eluted with 75 mL of n-hexane-ether mixed solvent (volume ratio 9:1), followed by elution of polar compounds with 75 mL of ether. The eluted solvents were collected, evaporated to dryness, and dried in an oven at 110 °C to constant weight which represent the weight of the total polar compound.

2.7.2. AOL@ZIF-8 catalyzed transesterification of used cooking oil for production of biodiesel

AOL@ZIF-8 was used to catalyze transesterification of used cooking oil (produced in 2.7.1) for production of biodiesel in a jacketed glass reactor. Briefly, 5 g of used cooking oil was mixed with methanol (alcohol-to-oil molar ratio of 6:1), and water (10 wt % of used cooking oil). AOL@ZIF-8 (2.5 wt % of used cooking oil) was added to initiate the transesterification reaction. The reaction mixture was stirred at 200 rpm and kept at 40 °C for 12 h. At the end of the reaction, the reaction mixture was centrifuged (10,000 g for 10 min) to separate the AOL@ZIF-

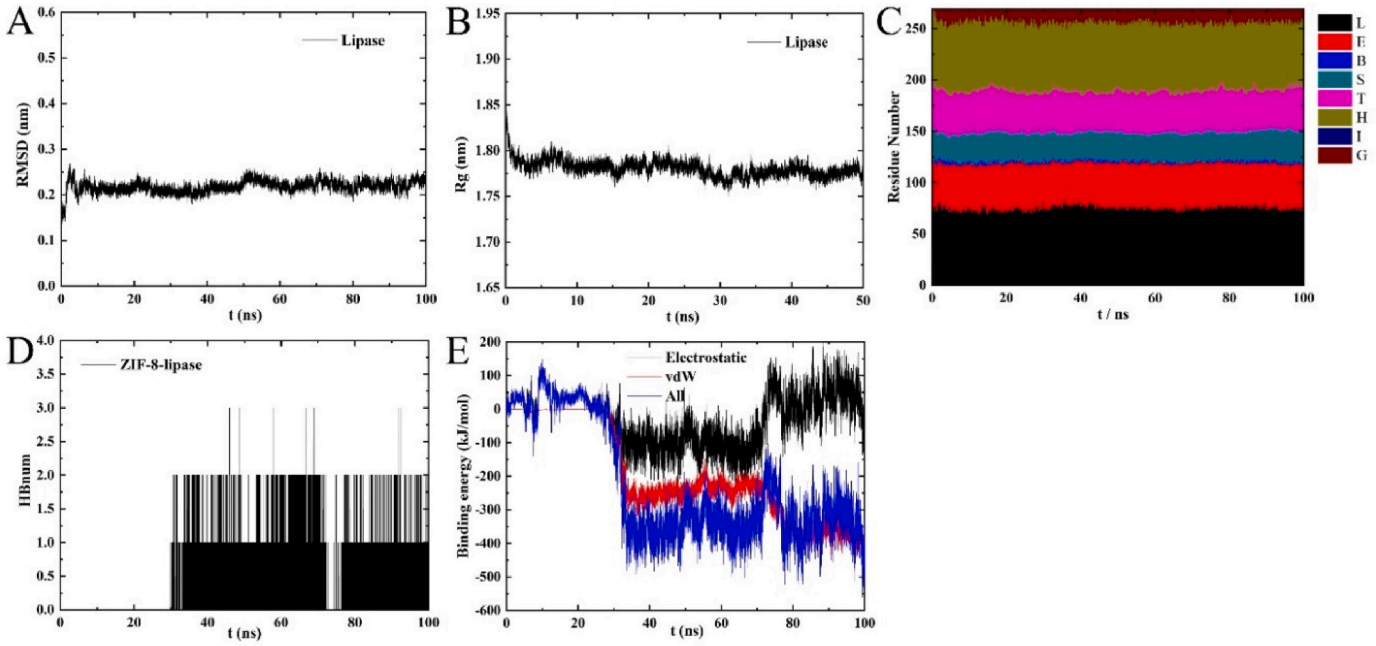

Fig. 2. RMSD (A), Rg (B) and number of residues involved in the secondary structure (C) of AOL during the simulation; Number of hydrogen bond (D) and interaction force (E) between AOL and ZIF-8.

8 from reaction product. The collected AOL@ZIF-8 was reused in five consecutive transesterification reactions. The resultant biodiesel was mixed with internal standard solution (800 μL heptadecanoic acid methyl ester n-hexane solution, 2.5 mg/mL) and quantified using GC-FID (Shimadzu, GC-2030) equipped with a CP-Sil 88 capillary column (100 m × 0.25 mm × 0.20 μm). The initial column temperature was set at 45 °C and held for 4 min, heated to 175 °C at a rate of 13 °C/min and held for 27 min, and finally heated to 215 °C at a rate of 4 °C/min and held for 35 min. FAME content was calculated by Equation (4):

$$\text{FAME content}\ (\%) = \frac{m_i \times As}{m_S \times A_i} \times 100 \tag{4}$$

where m_i and m_s represent the mass of internal standard and sample, respectively; A_i and A_s represent peak area of internal standard and FAMEs, respectively [23]. The density of biodiesel was measured by METTLER TOLEDO D4 and the viscosity was measured by HAAKE MARS 40 Rheometer.

3. Results and discussion

3.1. Molecular simulation of the adsorption behavior of AOL onto ZIF-8

MD simulation was applied to understand the adsorption behavior of AOL onto ZIF-8. Fig. 1A and B showed the distance and contact area between AOL and ZIF-8 over the course of a 100 ns simulation. Initially (0 ns), free AOL and ZIF-8 were separated by a distance of 5 nm with no contact area. At 20 ns, free AOL began to approach ZIF-8 and establish stable binding by 35 ns. At this point, a notable decrease in distance

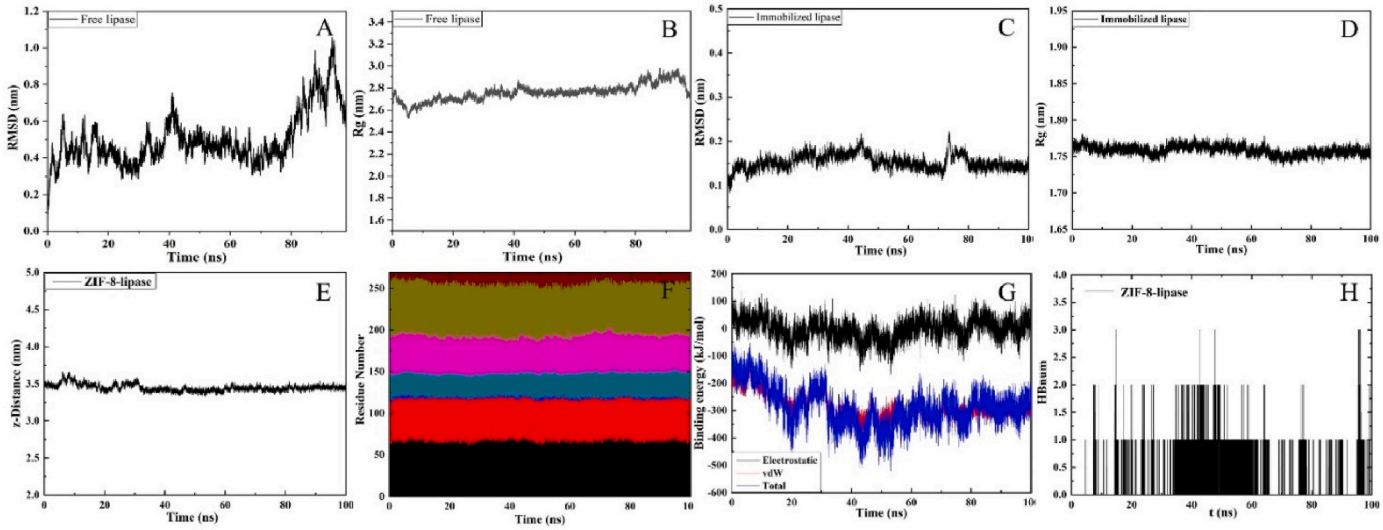

Fig. 3. RMSD (A) and Rg (B) of free AOL in methanol solution; RMSD (C), Rg (D) of immobilized AOL; Distance between AOL and ZIF-8 in methanol solution (E); Number of residues involved in the secondary structure of AOL (F); Interaction force (G) and number of hydrogen bond (H) between AOL and ZIF-8 during the MD simulation.

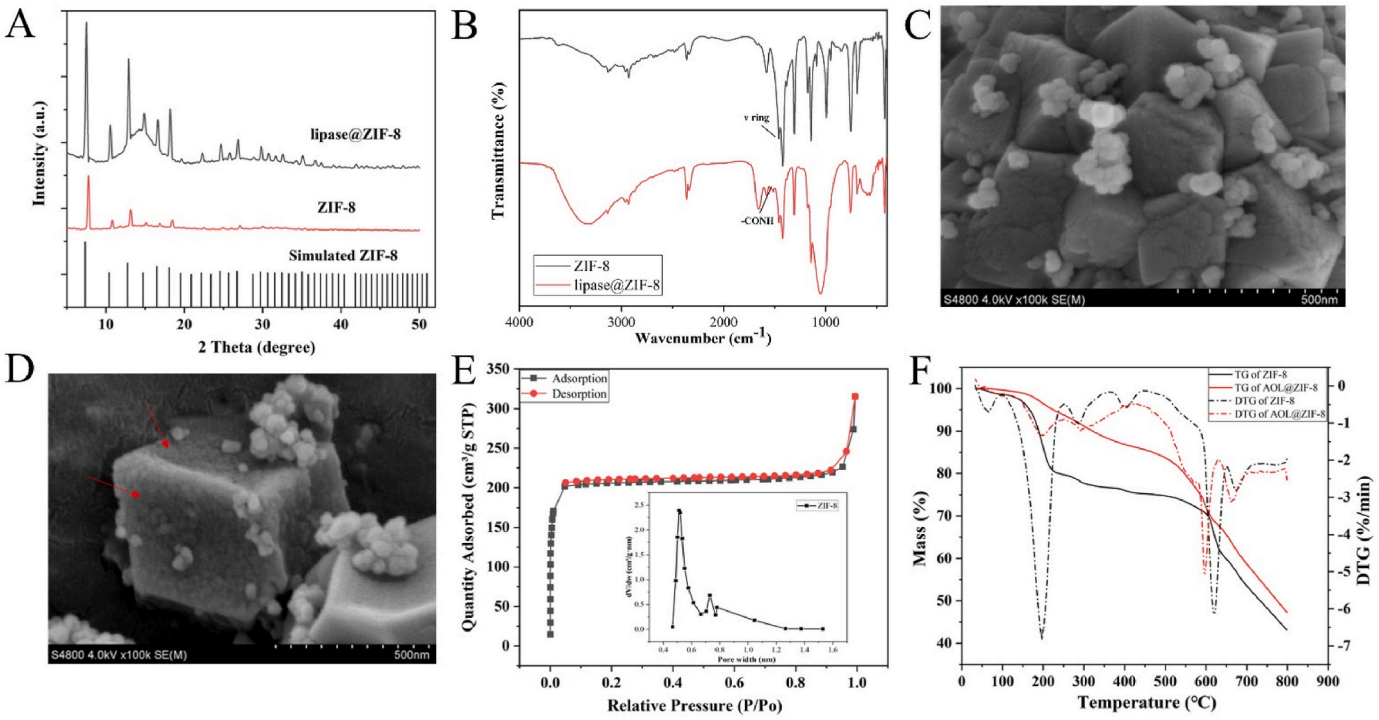

Fig. 4. XRD of ZIF-8, AOL@ZIF-8 and simulated ZIF-8 (A); FTIR of ZIF-8 and AOL@ZIF-8 (B); SEM images of ZIF-8 (C) and AOL@ZIF-8 (D); BET of ZIF-8 (E) and TGA curves of ZIF-8 and AOL@ZIF-8 (F).

(3.127 nm) and a significant increase in contact area (6.437 nm^2) between AOL and ZIF-8 were observed (Fig. 1A and B). Subsequently, the contact area between free AOL and ZIF-8 further expanded to 9.835 nm^2 by 75 ns, indicating a stronger adsorption of AOL onto the surface of ZIF-8. This was accompanied by a reduction in distance between AOL and ZIF-8 to 2.992 nm at 75 ns (Fig. 1A and B). A 3D schematic diagram of the AOL and ZIF-8 structures revealed that Lys279 at the carbonyl end of the protein entered the pores of ZIF-8 at 75 ns, leading to enhanced contact area and reduced centroid distance between ZIF-8 and lipase (Fig. 1C).

We further explored the impact of AOL binding onto ZIF-8 on the dynamic behavior and conformational changes of AOL. The dynamic behavior of the enzyme was assessed using root mean square deviation (RMSD), an essential indicator for assessing simulation system convergence and describing differences in conformation between the system and the target conformation [24]. Fig. 2A illustrates the variation of the RMSD of the Cα atom of lipase over time. Throughout the entire simulation period, the structure of AOL remained stable, with an average RMSD value of 0.2183 nm.

The radius of gyration (Rg), which reflects the degree of molecular expansion indicates the stability of enzyme protein. As shown in Fig. 2B, AOL exhibited minimal expansion, with an average Rg value of 1.7765 nm, indicating structural stability throughout the simulation process. Furthermore, the number of residues in the secondary structures of AOL remained unchanged throughout the simulation (Fig. 2C), suggesting that the adsorption of AOL onto the surface of ZIF-8 did not alter the conformation of AOL. This agrees with previous study that shows minimal changes in the natural conformation of *Candida rugosa* lipase (CRL) following adsorption of CRL onto ZIF-8. Presence of water molecules within the pores of ZIF-8 has helped to maintain the natural conformation of CRL [25].

We also examined the adsorption mechanism of AOL onto ZIF-8. ZIF-8 contains amine groups and nitrogen atoms that can act as hydrogen bond donors or acceptors [26]. During the MD simulation, the number of hydrogen bonds formed between AOL and ZIF-8 increased from 0 to 3 (Fig. 2D). In addition to hydrogen bonding, electrostatic and van der Waals interactions were observed between AOL and ZIF-8 (Fig. 2E). The average electrostatic and van der Waals interaction energies gradually decreased throughout the simulation, indicating formation of stable binding between AOL and ZIF-8. Stable binding was established at 35 ns, with electrostatic interaction and van der Waals interaction energies of −371.62 and −340.58 kJ/mol, respectively.

3.2. Molecular simulation of the methanol tolerance of AOL@ZIF-8

Methanol tolerance of free AOL and AOL@ZIF-8 were investigated using a 100 ns molecular simulation in 10 % methanol solution. Free AOL in the methanol solution exhibited significant fluctuations in RMSD (Fig. 3A) and Rg (Fig. 3B) values, indicating structural changes of free AOL in the presence of methanol. Similar observations were reported by Sandaka and colleagues. Methanol-water systems induced lipase denaturation leading to alterations in RMSD and Rg values [27]. In contrast, AOL@ZIF-8 exhibited minimal changes in RMSD and Rg values in the methanol solution, indicating immobilization of AOL onto ZIF-8 surfaces enhanced the structural stability of AOL@ZIF-8 in methanol solution (Fig. 3C and D). Furthermore, the distance between AOL and ZIF-8 remained constant at 3.447 nm throughout the simulation process, suggesting that methanol solution had no effect on AOL leaching, and AOL remained adsorbed onto ZIF-8 (Fig. 3E). The secondary structure of AOL@ZIF-8 in the methanol solution remained stable (Fig. 3F). The binding energy between lipase and ZIF-8 during the simulation process is depicted in Fig. 3G. The average electrostatic interaction energy, van der Waals interaction energy, and total interaction energy of ZIF-8 and lipase were 15.26, −296.05, and −280.79 kJ/mol, respectively. Compared to the binding energy of AOL and ZIF-8 in water, the interaction between ZIF-8 and lipase weakened in the presence of methanol. The number of hydrogen bonds formed between AOL and ZIF-8 varied between 0 and 3, indicating the stability of the AOL-ZIF-8 composite structure (Fig. 3H).

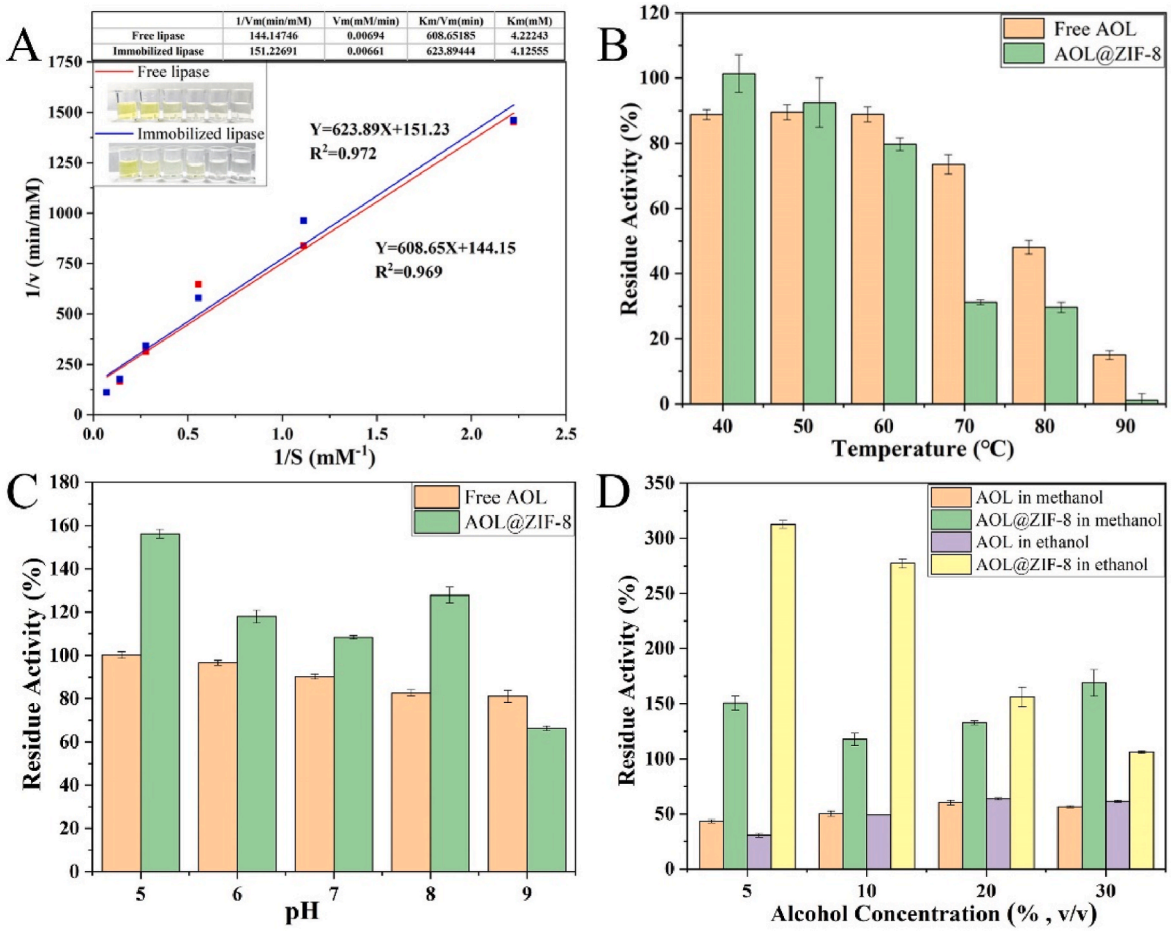

Fig. 5. Kinetic parameters (Km and Vmax) of free AOL and AOL@ZIF-8 (A); Thermal (B), pH (C) and alcohol stability (D) of free AOL and AOL@ZIF-8.

3.3. Synthesis and characterization of ZIF-8 and AOL@ZIF-8

AOL was successfully immobilized on ZIF-8 with an immobilization efficiency of 64.71 % and a protein loading of 57.36 mg/g. Usually, there are multiple factors that affect the efficiency of lipase immobilization and the amount of protein immobilized, including lipase concentration, immobilization time and temperature, and the hydrophilic/hydrophobic nature of the carrier surface. Fig. 4A shows the XRD patterns of ZIF-8 and AOL@ZIF-8. The characteristic peaks observed for ZIF-8 and AOL@ZIF-8 were in agreement with the simulated ZIF-8 pattern, indicating successful synthesis of ZIF-8 and that the immobilization of AOL onto ZIF-8 did not affect crystallinity of the ZIF-8 structure. The chemical structure of ZIF-8 and AOL@ZIF-8 were further investigated using FTIR (Fig. 4B). Absorption peaks at 420 cm^{-1} and 1500–1350 cm^{-1} (v ring) corresponded to the vibration of Zn-N and the vibration of HmIM, respectively, indicating presence of Zn^{2+} and 2-methylimidazole in ZIF-8 and AOL@ZIF-8 [10]. Additionally, AOL@ZIF-8 had an absorption peak at 1600-1700 cm^{-1}, corresponding to the stretching vibration of -CONH in protein (amide I region) [28], indicating the successful immobilization of AOL onto ZIF-8. The morphology of the ZIF-8 and AOL@ZIF-8 was observed using SEM. SEM images revealed that both ZIF-8 (Fig. 4C) and AOL@ZIF-8 (Fig. 4D) exhibited clear polyhedral morphology, with dimensions of approximately 350 nm. The porosity of ZIF-8 was characterized using nitrogen adsorption experiments. Fig. 4E depicts type I isotherms. The BET surface area of ZIF-8 was determined to be 868.3210 m^2/g, with a median pore width of 0.5502 nm according to the Horvath-Kawazoe method. Considering the molecular dimensions of AOL (4.73 nm × 6.72 nm × 8.95 nm), AOL was adsorbed onto the surface of ZIF-8 rather than encapsulated within the pores. Fig. 4F displays the thermogravimetric analysis of ZIF-8 and AOL@ZIF-8. ZIF-8 exhibited only slight weight loss at 160 °C, which attributed to the loss of solvent molecules. Subsequently, a plateau was observed at temperatures ranging from 200 °C to 600 °C, indicating the thermostability of ZIF-8. The rapid mass loss observed after 600 °C corresponded to the thermal decomposition of ZIF-8. Notably, a weight loss of 7.47 % was observed at 292 °C in the TGA curve of AOL@ZIF-8, which aligned with pyrolysis of lipase molecules [29], further confirming the successful adsorption of AOL onto ZIF-8.

3.4. Catalytic activity and stability of free AOL and AOL@ZIF-8

Free AOL exhibited a transesterification activity of 215.5 ± 1.623 U/g, meanwhile AOL@ZIF-8 demonstrated a slightly higher activity of 228.554 ± 9.291 U/g. The activity recovery of AOL@ZIF-8 was calculated to be 106.18 ± 6.97 %. As MD simulation results shows minimal change in the secondary structure of AOL following immobilization, the transesterification activity of AOL@ZIF-8 could be retained. Fig. 5A shows the kinetic parameters (Km and Vmax) of both free AOL and AOL@ZIF-8. Both AOL (0.0066 mM/min) and AOL@ZIF-8 (0.0069 mM/min) exhibited similar Vmax values. However, the Km value of AOL@ZIF-8 (4.125 mM) was slightly lower than that of free AOL (4.222 mM), indicating a higher affinity of AOL@ZIF-8 for the substrate.

In terms of catalytic stability, AOL@ZIF-8 exhibited higher catalytic activity compared to free AOL after thermal treatment at 40 °C and 50 °C for 30 min, indicating that immobilization can improve thermal stability (Fig. 5B). However, both AOL@ZIF-8 and free AOL showed rapid decline in catalytic activity following exposure to temperatures above 70 °C,

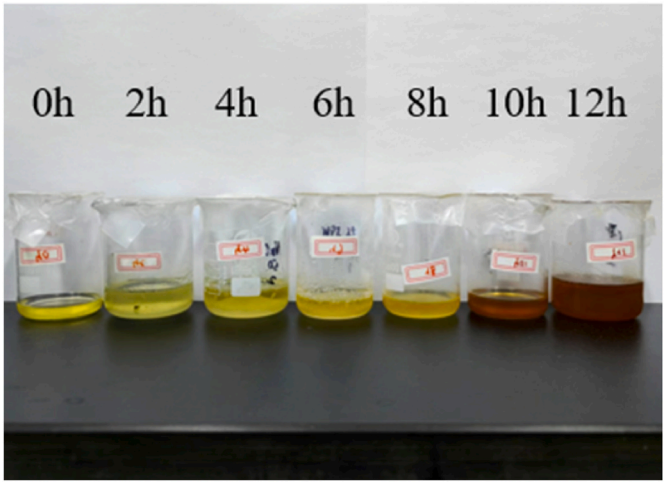

Fig. 6. Visual representation of used cooking oil with different frying time.

which corresponding to the deactivation of lipase at high temperatures. Regarding pH stability, AOL@ZIF-8 demonstrated superior pH stability as compared to free AOL in acidic and basic environments (pH from 5 to 9) (Fig. 5C) indicating enhanced resistance of AOL@ZIF-8 to acidity, which is advantageous for biodiesel production using acidic feedstocks. Furthermore, AOL@ZIF-8 exhibited higher catalytic activity in the presence of 5 %–30 % methanol and ethanol as compared to free AOL (Fig. 5D), with a more pronounced effect at lower alcohol concentrations (5 % and 10 %). The catalytic activity of AOL@ZIF-8 increased by up to 1.5 times in 5 % methanol and 3.13 times in 5 % ethanol, respectively.

The secondary structures of AOL@ZIF-8 following treatment in alcohol solutions were analyzed using FT-IR. Following methanol treatment, the α-helix content decreased from 18.26 ± 2.42 % to 16.92 ± 3.21 %, meanwhile the β-sheet content increased from 19.35 ± 1.12 % to 23.08 ± 5.2 %. Similar changes in secondary structure content were observed in ethanol-treated AOL@ZIF-8. Decreased in α-helix structure and increased in β-sheet structure has been reported to lead to an "open" conformation in lipase which can enhance the catalytic activity of AOL@ZIF-8 [30].

3.5. Effects of frying time on the acid value, peroxide value and total polar compound of the used cooking oils

Fig. 6 shows the change in the color of the used cooking oil with frying time. The color of the used cooking oil changed from transparent light yellow to turbid dark brown with increased frying time (from left to right).

The acid value, peroxide value, and total polar compound content of the used cooking oil at different frying times are shown in Fig. 7A–C. Acid value of the used cooking oil increased rapidly in the first 8 h from 0.84 mg KOH/g to 2.19 mg KOH/g (Fig. 7A). At 12 h, the acid value for used cooking oil was 2.25 mg KOH/g, which did not exceed the requirement stipulated by China's National Food Safety Standard for Edible Vegetable Oils (acid value of edible oil of ≤5 mg KOH/g).

Peroxide value reflects the content of hydroperoxides generated in the initial stage of lipid oxidation. Peroxide value of the used cooking oil increased from 0.0145 g/100g at 0 h to 0.1465 g/100g at 12 h (Fig. 7B). This is in agreement with previously reported findings which found increasing peroxide value with frying time [31]. Total polar compounds are polar substances generated during repeated frying process. According to China's National Food Safety Standard for Edible Vegetable Oils, the total polar compound content of edible oil should not exceed 27 %. After 12 h of repeated frying, total polar compound in used cooking oil was 27.53 % (Fig. 7C). Increased in the acid value, peroxide value and total polar compound after 12 h of repeated frying are indication of quality deterioration of the cooking oil. Presence of free fatty acids, aldehydes, ketones and polar compounds in the used cooking oil will affect stability of lipases.

3.6. AOL@ZIF-8 catalyzed transesterification of used cooking oil for production of biodiesel

When free AOL was used as the catalyst, the yield was also low (1.08 %) which may be due to the high acid value of the used cooking oil

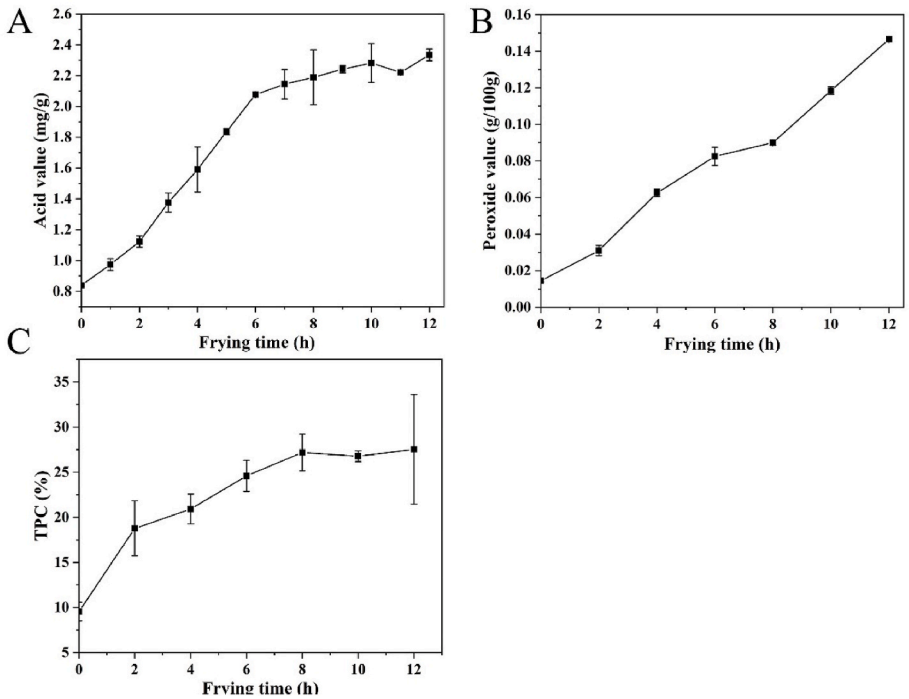

Fig. 7. Acid value (A), peroxide value (B) and total polar compound content (C) of the used cooking oil.

Table 1
Biodiesel preparation with ZIF-immobilized lipase.

Source of lipase	Immobilization method	Support	Feedstock	Reaction parameters (Methanol to oil molar ratio/reaction time/temperature)	Yield/ %	Reusability	Reference
Aspergillus niger	diffusion	macroporous ZIF-8	soybean oil	4:1/12 h/45 °C	80	68 % after 5 cycles	[23]
Aspergillus niger	diffusion	hydrophobic macroporous ZIF-8	soybean oil	4:1/24 h/45 °C	88	96 % after 5 cycles	[32]
Thermomyces lanuginosus	diffusion	magnetic macroporous ZIF-8	soybean oil	46 μL/12 h/40 °C	98.96	93.5 % after 5 cycles	[33]
Candida rugosa	encapsulation	ZIF-8	hemp oil	6:1/48 h/50 °C	75	80 % after 5 cycles	[9]
Candida Rugosa	adsorption	Fe_3O_4@ZIF-8	waste oil	6:1 mmol/g/2 h/40 °C	82.06	74.52 % after 3 cycles	[34]
Candida Antarctica	adsorption	ZIF-8	African palm oil	12:1/8 h/45 °C	93.4	60 % after 3 cycles	[10]
Aspergillus oryzae	adsorption	phthalic acid-ZIF-8	soybean oil	460 μL/12 h/40 °C	80	81.5 % after 5 cycles	[35]
Eversa Transform 2.0	encapsulation	ZIF-8	microalgal oil	0.2 mL/3 h/45 °C	56.1	32.5 % after 5 cycles	[36]
Aspergillus oryzae	adsorption	ZIF-8	used cooking oil	6:1/12 h/40 °C	81.19	68.46 % after 5 cycles	this work

affecting the activity of the free lipase. In contrast, AOL@ZIF-8 showed better catalytic performance. After 12 h of reaction time, AOL@ZIF-8 are successfully used to catalyze transesterification of used cooking oil (acid value of 2.25 mg KOH/g, peroxide value of 0.1465 g/100g and TPC of 27.53 %) for production of biodiesel (FAME content of 81.19 %). Compared to 96.5 % of ester content in standard EN 14214, the pretreatment of used cooking oil, along with the purification and refinement processes applied to the biodiesel samples, could contribute to improving the FAME content observed in this study, which was 81.19 %. The density of biodiesel (FAME content of 80.17 %) was 0.892 g/cm^3 and the viscosity was 8.02 mm^2/s at 25 °C. After five consecutive transesterification, AOL@ZIF-8 retained 68.46 % of its initial yield. This is probably due to leakage of the AOL adsorbed on the surface of ZIF-8 [10].

To compare the results of this study with other works, Table 1 lists recent literature on the preparation of biodiesel using ZIF-8 immobilized lipases.

4. Conclusion

Results from the MD simulation show that AOL are adsorbed onto the surface of ZIF-8 via hydrogen bonding, electrostatic interaction and van der Waals interaction with minimal changes to its native configurations. Moreover, MD simulations showed AOL@ZIF-8 can maintain its structure in methanol solutions as compared to free AOL. AOL was successfully immobilized on ZIF-8 with an immobilization efficiency of 64.71 %. AOL@ZIF-8 demonstrated slightly higher transesterification activity than free AOL with an activity recovery of 106.18 %. In agreement with MD simulations, AOL@ZIF-8 exhibited enhanced stability in wide range of pH and under presence of alcohol solution. AOL@ZIF-8 can be used to catalyze transesterification of used cooking oil for production of biodiesel (FAME content of 81.19 %).

CRediT authorship contribution statement

Shuaibo Xia: Writing – original draft, Methodology, Investigation, Data curation. **Cai Shen:** Writing – review & editing, Data curation. **Jiale Lin:** Investigation, Formal analysis. **Maolin Tu:** Writing – review & editing, Conceptualization. **Chin-Ping Tan:** Writing – review & editing, Conceptualization. **Ling-Zhi Cheong:** Writing – review & editing, Funding acquisition, Data curation, Conceptualization.

Declaration of competing interest

The authors declare that they have no known competing financial interests or personal relationships that could have appeared to influence the work reported in this paper.

Acknowledgement

This work was sponsored by Key R&D Program of Zhejiang Province (2022C04009, China) and National Natural Science Foundation of China (21706137).

References

[1] E. Parandi, M. Safaripour, M.H. Abdellattif, M. Saidi, A. Bozorgian, H.R. Nodeh, S. Rezania, Biodiesel production from waste cooking oil using a novel biocatalyst of lipase enzyme immobilized magnetic nanocomposite, Fuel 313 (2022) 123057.
[2] S. Xia, J. Lin, S. Sayanjali, C. Shen, L.-Z. Cheong, Lipase-catalyzed production of biodiesel: a critical review on feedstock, enzyme carrier and process factors 18 (1) (2024) 291–309.
[3] N. Binhayeeding, S. Klomklao, P. Prasertsan, K. Sangkharak, Improvement of biodiesel production using waste cooking oil and applying single and mixed immobilised lipases on polyhydroxyalkanoate, Renew. Energy 162 (2020) 1819–1827.
[4] X. Zhao, F. Qi, C. Yuan, W. Du, D. Liu, Lipase-catalyzed process for biodiesel production: enzyme immobilization, process simulation and optimization, Renew. Sustain. Energy Rev. 44 (2015) 182–197.
[5] Y. Shi, H. Zhou, L. Dai, D. Liu, W. Du, Preparation of ordered macroporous ZIF-8-derived magnetic carbon materials and its application for lipase immobilization 14 (1) (2024) 55.
[6] Y. Cheng, B. Ma, C.-P. Tan, O.-M. Lai, W. Panpipat, L.-Z. Cheong, C.J.S. Shen, A. B. Chemical, Hierarchical Macro-Microporous ZIF-8 Nanostructures as Efficient Nano-Lipase Carriers for Rapid and Direct Electrochemical Detection of Nitrogenous Diphenyl Ether Pesticides, vol. 321, 2020 128477.
[7] J. Lin, Y. Cheng, i. La, Oi-Ming, C.P. Tan, W. Panpipat, C. Shen, L.Z. Cheong, Biomimetic mineralization of metal ion-doped lipase into ZIF-8 framework for enhanced hydrolytic activity in biphasic system, ChemistrySelect 7 (38) (2022) e202202721.
[8] B. Ma, L.-Z. Cheong, X. Weng, C.-P. Tan, C. Shen, Lipase@ZIF-8 nanoparticles-based biosensor for direct and sensitive detection of methyl parathion, Electrochim. Acta 283 (2018) 509–516.
[9] F. Zha, M. Shi, H. Li, J. Rao, B. Chen, Biomimetic mineralization of lipase@MOF biocatalyst for ease of biodiesel synthesis: structural insights into the catalytic behavior, Fuel 357 (2024) 129854.
[10] L. Giraldo, F. Gómez-Granados, J.C. Moreno-Piraján, Biodiesel production using palm oil with a MOF-lipase B biocatalyst from Candida Antarctica: a kinetic and thermodynamic study 24 (13) (2023) 10741.
[11] X. Hu, Z. Zeng, J. Zhang, D. Wu, H. Li, F. Geng, Molecular dynamics simulation of the interaction of food proteins with small molecules, Food Chem. 405 (2023) 134824.
[12] D. Zhao, C. Peng, J. Zhou, Lipase adsorption on different nanomaterials: a multi-scale simulation study, Phys. Chem. Chem. Phys. 17 (2) (2015) 840–850.
[13] J.A. Maier, C. Martinez, K. Kasavajhala, L. Wickstrom, K.E. Hauser, C. Simmerling, ff14SB: improving the accuracy of protein side chain and backbone parameters from ff99SB, J. Chem. Theor. Comput. 11 (8) (2015) 3696–3713.
[14] B. Zheng, M. Sant, P. Demontis, G.B. Suffritti, Force field for molecular dynamics computations in flexible ZIF-8 framework, J. Phys. Chem. C 116 (1) (2012) 933–938.

[15] S. Nosé, M. Klein, Constant pressure molecular dynamics for molecular systems, Mol. Phys. 50 (5) (1983) 1055–1076.
[16] G. Bussi, D. Donadio, M. Parrinello, Canonical sampling through velocity rescaling, J. Chem. Phys. 126 (1) (2007) 014101.
[17] J. Wang, W. Wang, P.A. Kollman, D.A.J.J.o.m.g. Case, modelling, Automatic atom type and bond type perception in molecular mechanical calculations 25 (2) (2006) 247–260.
[18] J. Wang, R.M. Wolf, J.W. Caldwell, P.A. Kollman, D.A.J.J.o.c.c. Case, Development and testing of a general amber force field 25 (9) (2004) 1157–1174.
[19] T. Lu, F. Chen, Multiwfn: a multifunctional wavefunction analyzer, J. Computat. Chem. 33 (5) (2012) 580–592.
[20] M. Schauperl, P.S. Nerenberg, H. Jang, L.-P. Wang, C.I. Bayly, D.L. Mobley, M.K.J. C.c. Gilson, Non-bonded force field model with advanced restrained electrostatic potential charges (RESP2) 3 (1) (2020) 44.
[21] Y. Cheng, O.-M. Lai, C.-P. Tan, W. Panpipat, L.-Z. Cheong, C. Shen, Proline-modified UIO-66 as nanocarriers to enhance Candida rugosa lipase catalytic activity and stability for electrochemical detection of nitrofen, ACS Appl. Mater. Interfaces 13 (3) (2021) 4146–4155.
[22] C. Cheng, C. Shen, O.-M. Lai, C.-P. Tan, L.-Z. Cheong, Biomimetic self-assembly of lipase-zeolitic imidazolate frameworks with enhanced biosensing of protox inhibiting herbicides, Anal. Methods 13 (42) (2021) 4974–4984.
[23] Y. Hu, H. Zhou, L. Dai, D. Liu, S. Al-Zuhair, W. Du, Lipase immobilization on macroporous ZIF-8 for enhanced enzymatic biodiesel production, ACS Omega 6 (3) (2021) 2143–2148.
[24] J. Zhang, X. Chen, P. Lv, W. Luo, Z. Wang, J. Xu, Z. Wang, Bionic-immobilized recombinant lipase obtained via bio-silicification and its catalytic performance in biodiesel production, Fuel 304 (2021) 121594.
[25] H. He, L. Li, Y. Wu, D. Zhao, J. Liu, J. Zhou, Simulation insights into the lipase adsorption on zeolitic imidazolate framework-8, Colloids Surf. B Biointerfaces 231 (2023) 113540.
[26] H. Dai, X. Yuan, L. Jiang, H. Wang, J. Zhang, J. Zhang, T. Xiong, Recent advances on ZIF-8 composites for adsorption and photocatalytic wastewater pollutant removal: fabrication, applications and perspective, Coord. Chem. Rev. 441 (2021) 213985.
[27] B.P. Sandaka, J. Kumar, J.S. Melo, Mitigation of methanol inactivation of lipases by reaction medium engineering with glycine betaine for enzymatic biodiesel synthesis, Fuel 313 (2022) 122637.
[28] L. Zhong, Y. Feng, H. Hu, J. Xu, Z. Wang, Y. Du, J. Cui, S. Jia, Enhanced enzymatic performance of immobilized lipase on metal organic frameworks with superhydrophobic coating for biodiesel production, J. Colloid Interface Sci. 602 (2021) 426–436.
[29] G. Kuang, Z. Wang, X. Luo, Z. Geng, J. Cui, M. Bilal, Z. Wang, S. Jia, Immobilization of lipase on hydrophobic MOF synthesized simultaneously with oleic acid and application in hydrolysis of natural oils for improving unsaturated fatty acid production, Int. J. Biol. Macromol. 242 (2023) 124807.
[30] I.V. Pavlidis, D. Gournis, G.K. Papadopoulos, H. Stamatis, Lipases in water-in-ionic liquid microemulsions: structural and activity studies, J. Mol. Catal. B Enzym. 60 (1) (2009) 50–56.
[31] A. Waghmare, S. Patil, J.G. LeBlanc, S. Sonawane, S.S. Arya, Comparative assessment of algal oil with other vegetable oils for deep frying, Algal Res. 31 (2018) 99–106.
[32] Y. Hu, L. Dai, D. Liu, W. Du, Hydrophobic pore space constituted in macroporous ZIF-8 for lipase immobilization greatly improving lipase catalytic performance in biodiesel preparation, Biotechnol. Biofuels 13 (1) (2020) 1–9.
[33] Y. Li, H. Zhou, L. Dai, D. Liu, S. Al-Zuhair, W. Du, Immobilization of lipase from thermomyces lanuginosus in magnetic macroporous ZIF-8 improves lipase reusability in biodiesel preparation, ACS Omega 7 (1) (2022) 274–280.
[34] X. Hao, X. Zheng, Q. Zhang, X. Da, Y. Wang, Preparation of biodiesel catalyzed by immobilized lipase in magnetic ZIF-8 nanomaterial, Res. Chem. Intermed. (2024) 1–25.
[35] Z. Zou, H. Zhou, L. Dai, D. Liu, W.J.R.E. Du, A dual stable MOF constructed through ligand exchange for enzyme immobilization with improved performance in biodiesel, Production 208 (2023) 17–25.
[36] E. Sowan, H. Taher, M.S. Mozumder, S. Al-Zuhair, ZIF-8 as support for enhanced stability of immobilized lipase used with a thermoresponsive switchable solvent to simplify the microalgae-to-biodiesel process, Enzym. Microb. Technol. 167 (2023) 110243.